6th International Conference on Multiphase Flow,
ICMF 2007, Leipzig, Germany, July 9 – 13, 2007

Non-Isothermal Spreading of a Liquid Droplet with Dynamic Contact Angles on a Horizontal Surface

Sashikumaar Ganesan and Lutz Tobiska

Institute of Analysis and Numerical Computation

Otto-von-Guericke Universität,

PF4120, 39106 Magdeburg, Germany.

[ga.sashikumaar, tobiska]@mathematik.uni-magdeburg.de

Keywords: incompressible flow, heat transfer, moving contact line, finite elements, ALE approach

Abstract

A mathematical model for an non-isothermal liquid droplet deformation with dynamic contact angles on a horizontal solid surface is presented. The main challenges such as the inclusion of the contact angle in the model, prescribing the boundary condition at the moving contact line, Marangoni convection are addressed in our model. The solution is approximated by finite elements on moving meshes with arbitrary Lagrangian Eulerian (ALE) approach. The computational results show that the heat transfer slows down the spreading rate and the maximum value of the wetting diameter.

Introduction

Spreading of a droplet on a solid surface has been studied theoretically, numerically and experimentally by several authors. Apart from other difficulties in the numerical computation of free surface (Liquid-Gas interface) flows, deformation of droplets with dynamic contact angles posses additional difficulties. The main challenges in computations are the inclusion of dynamic contact angles, see for $e.g.$, Šikalo *et al.* (2005), the description of a boundary condition for the liquid velocity at the moving contact line, where the three phases (Liquid, Gas and Solid) intersect, see for $e.g.$, Dussan V (1976), and the variations in the surface tension due to changes in the local Liquid-Gas interface temperature.

The contact angle is an important property of a liquid droplet which is determined by the material properties of the liquid, solid and gas phases. Based on the contact angle, liquid droplets can be classified into wetting and non-wetting liquid droplets. This property plays a significant role in industrial applications. For instance, a small contact angle is desired in spray coolings, whereas a large contact angle is desired on self cleaning materials. Thus, the inclusion of the contact angle in the numerical computations is essential for producing physically relevant solutions. In the sequence of spreading and recoiling processes, often the contact angle *hysteresis* occurs on real surfaces. The difference between the advancing contact angle θ_a and the receding contact angle θ_r is generally referred to as the contact angle hysteresis. The advancing contact angle θ_a is the largest angle just before the spreading starts and the receding contact angle θ_r is the smallest angle just before the recoiling starts. Surface roughness, inhomogeneity and contaminations are a few reasons for the occurrence of the hysteresis. In our model we include the static contact angle in a weak sense allowing the hysteretic behaviour in the dynamic regime. For reducing the smoothness requirements, the curvature is replaced by the Laplace-Beltrami operator and integration by parts as described in Ganesan (2006).

Using the no-slip condition on the liquid-solid interface, the model leads to an non-integrable force singularity at the moving contact line, where the liquid-solid and liquid-gas interfaces intersect, see for $e.g.$ Hocking (1977). A few authors calls this singularity *"kinematic paradox"*, see for $e.g.$ Behr & Abraham (2002). Several boundary conditions have been proposed in the literature to relieve this singularity, see for an overview Eggers & Stone (2004). Among them, the so-called Navier-slip boundary condition has been more often used and is widely accepted. It reads:

$$\mathbf{u}\cdot\boldsymbol{\nu}_S = 0, \qquad \mathbf{u}\cdot\boldsymbol{\tau}_{i,S} = -\epsilon_\mu(\boldsymbol{\tau}_{i,S}\cdot\mathbb{T}(\mathbf{u},p)\cdot\boldsymbol{\nu}_S),$$

for $i = 1, ..., d-1$, where d is the dimension of the considered problem, $\boldsymbol{\nu}_S$ and $\boldsymbol{\tau}_{i,S}$ are the unit normal and tangential vectors on the liquid-solid interface. Here ϵ_μ is the slip coefficient. The unit of the stress is kg/(m·s^2) and of the velocity is m/s. Thus, from the dimensional analysis, the unit of the slip coefficient ϵ_μ should be of $\epsilon\mu_\epsilon^{-1}$, where ϵ and μ_ϵ have the unit of a length and a dynamic viscosity, respectively. The first condition is the no penetration boundary condition, that is, the fluid cannot penetrate an impermeable solid and thus the normal component of the velocity is zero. The second condition is the slip with friction boundary condition, that is, on the liquid-solid interface, the tangential velocities of the fluid are proportional to their corresponding tangential stresses.

Marangoni convection, which is a convection driven by

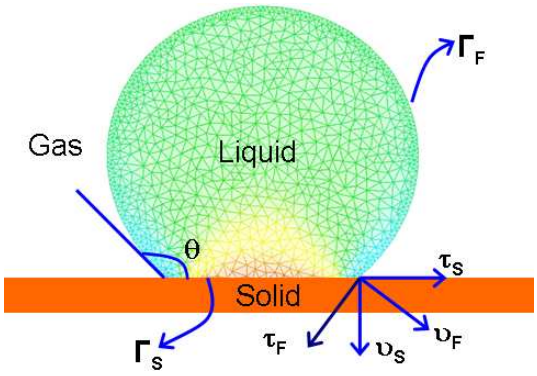

Figure 1: Non-isothermal liquid droplet on a horizontal surface.

variations in the surface tension along the Liquid-Gas interface Γ_F, is also considered in our model. We assume that the surface tension is linearly dependent on the temperature. Further, we assume that all material parameters such as density, viscosity and thermal conductivity in the droplet are independent of the temperature. In our model, the temperature of the solid surface is assumed to be below the boiling point temperature, and thus the Leidenfrost effect does not occur.

Continuous model

We consider a 3D-axisymmetric liquid droplet, which is in the atmospheric temperature, impinging on an uniformly heated horizontal surface. Figure 1 illustrates the computational domain of the droplet in 2D. In the figure, Γ_F and Γ_S are the liquid-gas and liquid-solid interfaces, respectively. Further, $\boldsymbol{\nu}_F$, $\boldsymbol{\nu}_S$ and $\boldsymbol{\tau}_F$, $\boldsymbol{\tau}_S$, denote the outward unit normal and tangential vectors on the corresponding interfaces. The droplet spreading is modeled as a one-phase flow neglecting the flow field in the gas-phase setting the pressure field constant in the surrounding gas. The fluid flow and the temperature fields in the liquid are described by the Navier-Stokes equations and the energy equation, respectively.

Marangoni convection

Marangoni convection is a convection driven by variations in the surface tension along the liquid-gas interface Γ_F. Since the surface tension is temperature dependent, these variations may occur due to the changes in the local surface temperature T on the liquid-gas interface Γ_F. In our model, we assume that the surface tension $\sigma(T)$ depends linearly on the temperature, more precisely

$$\sigma(T) = \sigma_0 - \mathcal{C}_1(T - T_{sa}). \tag{1}$$

Here, T_{sa} is the saturation temperature, σ_0 is the reference value of surface tension, and

$$\mathcal{C}_1 = -\frac{\partial \sigma}{\partial T}\Big|_{T=T_0} > 0$$

is the negative of rate of change of surface tension with respect to the temperature, see for $e.g.$, Anderson & Davis (1995). This relation induces thermocapillary effects in the fluid flow through the balance of shear stress with surface tension gradients along the liquid-gas interface Γ_F. Surface tension variations on the normal stress boundary condition are also considered in this study. We assume small buoyant forces, thus neglect natural convection phenomena.

Governing equations

The fluid flow in the droplet is governed by the time-dependent Navier-Stokes equation with the Marangoni convection in a time-dependent domain $\Omega(t) \subset \mathbb{R}^3$, t is the time. Further, the heat transfer in the droplet is described by the energy equation. In the time interval (0, I), where I is a given time, the Navier-Stokes equations and the energy equation together with the boundary conditions read:

$$\begin{aligned}
\frac{\partial \mathbf{u}}{\partial t} - \frac{1}{\rho}\nabla \cdot \mathbb{S}(\mathbf{u}, p) & & & \\
+(\mathbf{u}\cdot\nabla)\mathbf{u} &= g\mathbf{e} && \text{in } \Omega(t)\\
\nabla \cdot \mathbf{u} &= 0 && \text{in } \Omega(t)\\
\\
\mathbf{u}\cdot\boldsymbol{\nu}_F &= \mathbf{w}\cdot\boldsymbol{\nu}_F && \text{on } \Gamma_F(t)\\
\boldsymbol{\nu}_F\cdot\mathbb{S}(\mathbf{u},p)\cdot\boldsymbol{\nu}_F &= \sigma(T)\mathcal{K} && \text{on } \Gamma_F(t)\\
\boldsymbol{\tau}_{i,F}\cdot\mathbb{S}(\mathbf{u},p)\cdot\boldsymbol{\nu}_F &= \boldsymbol{\tau}_{i,F}\cdot\nabla\sigma(T) && \text{on } \Gamma_F(t)\\
\\
\mathbf{u}\cdot\boldsymbol{\nu}_S &= 0 && \text{on } \Gamma_S(t)\\
\epsilon_\mu(\boldsymbol{\tau}_{i,S}\cdot\mathbb{S}(\mathbf{u},p)\cdot\boldsymbol{\nu}_S) &= -\mathbf{u}\cdot\boldsymbol{\tau}_{i,S} && \text{on } \Gamma_S(t)\\
\\
\frac{\partial T}{\partial t} + (\mathbf{u}\cdot\nabla)T &= \frac{\lambda}{c_p\rho}\Delta T && \text{in } \Omega(t)\\
\\
-\lambda\frac{\partial T}{\partial \boldsymbol{\nu}_F} &= \alpha_F(T - T_\infty) && \text{on } \Gamma_F(t)\\
T &= T_w && \text{on } \Gamma_S(t)
\end{aligned} \tag{2}$$

with given $\Omega(0)$, $\mathbf{u}(0) = (0, 0, -u_{imp})$ and $T(0) = T_\infty$, for $i = 1, 2$. Here $\mathbf{u}$ denotes the velocity of the fluid, p the pressure in the fluid, T the temperature in the fluid, $\mathcal{K}$ is the sum of the principal curvatures, g the gravitational constant, $\mathbf{e}$ an unit vector in the opposite direction of the gravitational force and u_{imp} the impact speed of the droplet. Further, λ denotes the thermal conductivity, c_p the specific heat of the liquid, α_F the convection heat transfer coefficient on the liquid-gas interface, T_∞ the temperature of the surrounding gas and T_w is the given temperature at the hot surface.

The stress tensor $\mathbb{S}(\mathbf{u}, p)$ for Newtonian incompressible fluids is given by

$$\begin{aligned}
\mathbb{S}(\mathbf{u},p)_{i,j} &:= 2\mu\mathbb{D}(\mathbf{u})_{i,j} - p\delta_{i,j}\\
\mathbb{D}(\mathbf{u})_{i,j} &= \frac{1}{2}\left(\frac{\partial u_i}{\partial x_j} + \frac{\partial u_j}{\partial x_i}\right), \qquad i,j = 1,...,3,
\end{aligned}$$

where $\mathbb{D}(\mathbf{u})$ is the velocity deformation tensor and $\delta_{i,j}$ is the Kronecker delta. Note that, we used one of the possibilities of a boundary condition on the liquid-solid interface for the energy equation.

Variational form

For rewriting the model problem (2) in dimensionless form, we introduce the scaling factors L and U as characteristic length and velocity, respectively. Furthermore, we define the dimensionless variables as

$$\tilde{x} = \frac{x}{L}, \quad \tilde{\mathbf{u}} = \frac{\mathbf{u}}{U}, \quad \tilde{\mathbf{w}} = \frac{\mathbf{w}}{U}, \quad \tilde{t} = \frac{tU}{L},$$
$$\tilde{\mathrm{I}} = \frac{\mathrm{IU}}{L}, \quad \tilde{p} = \frac{p}{\rho U^2}, \quad \tilde{T} = \frac{T - T_\infty}{T_{sa} - T_\infty}.$$

Using these dimensionless variables in the stress tensor $\mathbb{S}(\mathbf{u}, p)$ and in the mass and momentum equations in (2), and omitting the tilde afterwards, we obtain the dimensionless form of the Navier-Stokes equations as

$$\begin{aligned} \frac{\partial \mathbf{u}}{\partial t} + (\mathbf{u}\cdot\nabla)\mathbf{u} - \nabla\cdot\mathbb{S}(\mathbf{u},p) &= \frac{1}{Fr}\,\mathbf{e} \quad \text{in } \Omega(t), \\ \nabla\cdot\mathbf{u} &= 0 \qquad \text{in } \Omega(t). \end{aligned} \tag{3}$$

The dimensionless form of the boundary conditions on the liquid-gas interface $\Gamma_F(t)$ in (2) reads:

$$\begin{aligned} \boldsymbol{\nu}_F\cdot\mathbb{S}(\mathbf{u},p)\cdot\boldsymbol{\nu}_F &= \frac{1}{We}\left(1 - \mathcal{C}\,(T-1)\right)\mathcal{K} \\ \boldsymbol{\tau}_{i,F}\cdot\mathbb{S}(\mathbf{u},p)\cdot\boldsymbol{\nu}_F &= -\frac{\mathcal{C}}{We}\,\boldsymbol{\tau}_{i,F}\cdot\nabla T, \end{aligned}$$

where $\mathcal{C} = \dfrac{\mathcal{C}_1(T_{sa} - T_\infty)}{\sigma_0}$.

The dimensionless form of the boundary conditions on the liquid-solid interface $\Gamma_S(t)$ in (2) read:

$$\begin{aligned} \mathbf{u}\cdot\boldsymbol{\nu}_S &= 0 \\ \beta_\epsilon(\boldsymbol{\tau}_{i,s}\cdot\mathbb{S}(\mathbf{u},p)\cdot\boldsymbol{\nu}_s) &= -\mathbf{u}\cdot\boldsymbol{\tau}_{i,s}. \end{aligned}$$

for $i = 1, 2$. Furthermore, the initial velocity becomes $\mathbf{u}(0) = (0, 0, -u_{imp})/U$, and in computations we use $U = u_{imp}$ to get $\mathbf{u}(0) = (0, 0, -1)$ and $L = r_0$, where r_0 is the radius of the droplet. Here, the dimensionless numbers (Reynolds, Weber, Froude and slip, respectively) are defined by

$$Re = \frac{\rho U L}{\mu}, \quad We = \frac{\rho U^2 L}{\sigma_0}, \quad Fr = \frac{U^2}{Lg}, \quad \beta_\epsilon = \epsilon_\mu \rho U.$$

Now, we derive the variational form of the dimensionless equations (3). To simplify the notation, we use the subscript t to represent the time dependency, for example, Ω_t for $\Omega(t)$. Let $L^2(\Omega_t)$ and $H^m(\Omega_t)$, $m \geq 1$ be the usual Lebesgue and Sobolev spaces. We define $Q = L^2(\Omega_t)$ as a pressure space and

$$V := \{\mathbf{v} \in H^1(\Omega_t)^3 : \mathbf{v}\cdot\boldsymbol{\nu}_S = 0 \ \text{ on } \Gamma_S(t)\}. \tag{4}$$

as a velocity space for (3). As a consequence, the no penetration boundary condition $\mathbf{u}\cdot\boldsymbol{\nu}_S = 0$ on the liquid-solid interface $\Gamma_S(t)$ will be satisfied in both the ansatz and test spaces. We include all other boundary conditions in the weak formulation. To get the weak formulation of the time dependent Navier-Stokes equations, we multiply the momentum and mass balance equations (3) by test functions $\mathbf{v} \in V$ and $q \in Q$, respectively, and integrate over Ω_t. By applying the Gaussian theorem for the stress tensor, we get the variational form of (3) as

For given $\Omega(0)$ and $\mathbf{u}(0)$, find $(\mathbf{u}(t), p(t)) \in V \times Q$ such that

$$\left(\frac{\partial \mathbf{u}}{\partial t}, \mathbf{v}\right) + a(\mathbf{u};\mathbf{u},\mathbf{v}) - b(p,\mathbf{v}) + b(q,\mathbf{u}) = f(\mathcal{K},\mathbf{v}), \tag{5}$$

for all $\mathbf{v} \in V$ and $q \in Q$. Here,

$$\begin{aligned} a(\hat{\mathbf{u}};\mathbf{u},\mathbf{v}) &= \frac{2}{Re}\int_{\Omega_t}\mathbb{D}(\mathbf{u}) : \mathbb{D}(\mathbf{v})\,dx + \int_{\Omega_t}(\hat{\mathbf{u}}\cdot\nabla)\mathbf{u}\cdot\mathbf{v}\,dx \\ &\quad + \frac{1}{\beta_\epsilon}\int_{\Gamma_{S_t}}(\mathbf{u}\cdot\boldsymbol{\tau}_{i,S})(\mathbf{v}\cdot\boldsymbol{\tau}_{i,S})\,d\gamma_S, \\ b(q,\mathbf{v}) &= \int_{\Omega_t} q\,\nabla\cdot\mathbf{v}\,dx, \\ f(\mathcal{K},\mathbf{v}) &= -\frac{1}{We}\int_{\Gamma_{F_t}}\left(1 - \mathcal{C}\,(T-1)\right)(\mathbf{v}\cdot\boldsymbol{\nu}_F)\mathcal{K}\,d\gamma_F \\ &\quad + \frac{\mathcal{C}}{We}\int_{\Gamma_{F_t}}(\mathbf{v}\cdot\boldsymbol{\tau}_{i,F})(\boldsymbol{\tau}_{i,F}\cdot\nabla T)\,d\gamma_F \\ &\quad + \frac{1}{Fr}\int_{\Omega_t}\mathbf{e}\cdot\mathbf{v}\,dx. \end{aligned}$$

Next, we derive the variational form of the energy equation. Using the dimensionless variables in the energy equation in (2), and omitting the tilde afterwards, we get the dimensionless form of the energy equation as

$$\frac{\partial T}{\partial t} + (\mathbf{u}\cdot\nabla)T - \frac{1}{Pe}\Delta T = 0 \quad \text{in } \Omega(t)\times(0,\mathrm{I}). \tag{6}$$

The energy boundary conditions on the liquid-gas and liquid-solid interfaces in (2) are transformed into the dimensionless form:

$$\begin{aligned} -\frac{\partial T}{\partial \boldsymbol{\nu}_F} &= Bi\,T \qquad \text{on } \Gamma_F(t) \\ T = T_D &= \frac{T_w - T_\infty}{T_{sa} - T_\infty} \quad \text{on } \Gamma_S(t). \end{aligned} \tag{7}$$

Here, *Pe* and *Bi* denote the dimensionless Peclet and Biot numbers, given by

$$Pe = \frac{LUc_p\rho}{\lambda}, \qquad Bi = \frac{\alpha_F L}{\lambda}.$$

Furthermore, the dimensionless initial temperature becomes $T(0) = 0$.

The weak form of the energy equation is obtained by multiplying it with a test function $\psi \in W$,

$$W := \{\psi \in H^1(\Omega_t) : \quad \psi = 0 \quad \text{on} \quad \Gamma_S(t)\},$$

and integration by parts. In particular, the diffusive term of the energy equation becomes

$$
\begin{aligned}
&-\frac{1}{Pe}\int_{\Omega_t}\Delta T\cdot\phi\,dx\\
&\quad=\frac{1}{Pe}\int_{\Omega_t}\nabla T:\nabla\phi\,dx-\frac{1}{Pe}\int_{\Gamma_{F_t}}\frac{\partial T}{\partial\boldsymbol{\nu}_F}\phi\,d\gamma_F\\
&\quad=\frac{1}{Pe}\int_{\Omega_t}\nabla T\cdot\nabla\phi\,dx+\frac{Bi}{Pe}\int_{\Gamma_{F_t}}T\,\phi\,d\gamma_F.
\end{aligned}
\tag{8}
$$

Hence, the weak form of the energy equation reads:

For given $\Omega(0)$ and $T(0)$, find $T(t)\in H^1(\Omega_t)$ with $T=T_D$ on Γ_{S_t} such that

$$
\left(\frac{\partial T}{\partial t},\phi\right)+a_T(\mathbf{u},T,\phi)+b_T(T,\phi)=0,
\tag{9}
$$

for all $\phi\in W$. Here,

$$
a_T(\mathbf{u},T,\phi)=\frac{1}{Pe}\int_{\Omega_t}\nabla T\cdot\nabla\phi\,dx+\int_{\Omega_t}(\mathbf{u}\cdot\nabla)\,T\,\phi\,dx,
$$

$$
b_T(T,\phi)=\frac{Bi}{Pe}\int_{\Gamma_{F_t}}T\,\phi\,dx.
$$

Inclusion of the contact angle

The contact angle is included by replacing the curvature $\mathcal{K}$ in the liquid-gas interface integral with the Laplace Beltrami operator and then integration by parts. This reduces one order of differentiation associated with the curvature term and increases one order of differentiation on the test function. A similar technique has been already employed in Ruschak (1980). The formulation by means of the Laplace Beltrami operator has been proposed in Dziuk (1991) and was also used in Bänsch (2001); Matthies (2002) for a closed liquid-gas interface flows, $i.e.$, flows without moving contact lines. In this paper, we extend this technique for flows with moving contact lines as follows

$$
\begin{aligned}
&\frac{1}{We}\int_{\Gamma_F(t)}(1-\mathcal{C}\,(T-1))\,\mathbf{v}\cdot\boldsymbol{\nu}_F\mathcal{K}\,d\gamma_F\\
&\quad=\frac{-1}{We}\int_{\Gamma_F(t)}(1-\mathcal{C}\,(T-1))\,\underline{\nabla}id_{\Gamma_F}:\underline{\nabla}\mathbf{v}\,d\gamma_F\\
&\qquad+\frac{1}{We}\int_{cl(t)}(1-\mathcal{C}\,(T-1))\,\boldsymbol{\nu}_{cl}\cdot\mathbf{v}\,d\zeta,
\end{aligned}
$$

since $\boldsymbol{\nu}_{cl}\cdot\underline{\nabla}id_{\Gamma_F}=\boldsymbol{\nu}_{cl}$. Here, $id_{\Gamma_F}:\mathbb{R}^d\mapsto\mathbb{R}^d$ is the identity, $\boldsymbol{\nu}_{cl}$ is the outward unit normal vector at the moving contact line $cl(t)$ with respect to the liquid-gas interface $\Gamma_F(t)$. Now, we decompose the test function in the contact line integral as

$$
\mathbf{v}=(\mathbf{v}\cdot\boldsymbol{\nu}_S)\boldsymbol{\nu}_S+\sum_{i=1}^{2}(\mathbf{v}\cdot\boldsymbol{\tau}_{i,S})\boldsymbol{\tau}_{i,S}
$$

and use the fact that $\mathbf{v}\cdot\boldsymbol{\nu}_S=0$ on Γ_S to get

$$
\begin{aligned}
&\int_{cl(t)}(1-\mathcal{C}\,(T-1))\,\boldsymbol{\nu}_{cl}\cdot\mathbf{v}\,d\zeta\\
&\quad=\int_{cl(t)}(1-\mathcal{C}\,(T-1))\,(\boldsymbol{\nu}_{cl}\cdot\boldsymbol{\tau}_{i,S})(\mathbf{v}\cdot\boldsymbol{\tau}_{i,S})\,d\zeta\\
&\quad=\int_{cl(t)}(1-\mathcal{C}\,(T-1))\cos(\theta)\;\mathbf{v}\cdot\boldsymbol{\tau}_{i,S}\,d\zeta,
\end{aligned}
\tag{10}
$$

since $\boldsymbol{\nu}_{cl}\cdot\boldsymbol{\tau}_{i,S}=\cos(\theta)$, where θ is the contact angle.

Numerical Scheme

The finite element method with the arbitrary Lagrangian Eulerian (ALE) approach is used to approximate the solution of (5). Here, we briefly recall the numerical scheme, for more details we refer to Ganesan (2006).

First, we semi-discretise the weak form in time using the fractional step-ϑ scheme. Next, we rewrite the semi-discrete form in an ALE form and linearise the non-linear convection term by an iteration of fixed point type. Further, we discretise the curvature term into a semi-implicit form as in Bänsch (2001). Then, we triangulate the domain by a triangular mesh and discretise the linear discrete equation in space by an inf-sup stable finite element pair P_2^{bubble}/P_1^{disc}, where the velocity is approximated by continuous, piecewise quadratic functions enriched with a cubic bubble function and the pressure is approximated by discontinuous, piecewise linear functions. The obtained system of linear algebraic equations is solved by the direct solver UMFPACK Davis & Duff (1997, 1999); Davis (2004).

To track the free surface, we move first the boundary points with the fluid velocity, and then displace the inner points with respect to the boundary displacement using elastic solid technique. We update the mesh in each sub-step of the fractional step-ϑ scheme and check the minium and maximum angle of each triangular element in the mesh. If any element violates the given minimum or maximum angle criteria, we remesh the domain with the same boundary/interface points and interpolate the solution to the new mesh from the old mesh. Due to the tangential movement, at some stage the boundary points may accumulate or the resolution of the boundary points become inadequate at some parts of the boundary. To overcome this difficulty we redistribute the boundary points using interpolated cubic splines when needed.

Results and Discussion

In this section, an array of computations is performed for a liquid droplet impinging on a hot solid surface. Here, we study the heat transfer in the droplet and the influence of the heat transfer on the wetting diameter. The validation of the model and the numerical scheme for an isothermal droplet deformation has been provided in Ganesan (2006). First, we present the shapes and wetting diameters of a droplet, which are numerically obtained with and without heat transfer. Next, we study the influence of the surface temperature on the wetting diameter. In all our computations, we use $C=1$ in the surface tension temperature relation. Another, important coefficient in these computations is the slip number β_ϵ, where we used a fixed value of 10^{-3} in all cases.

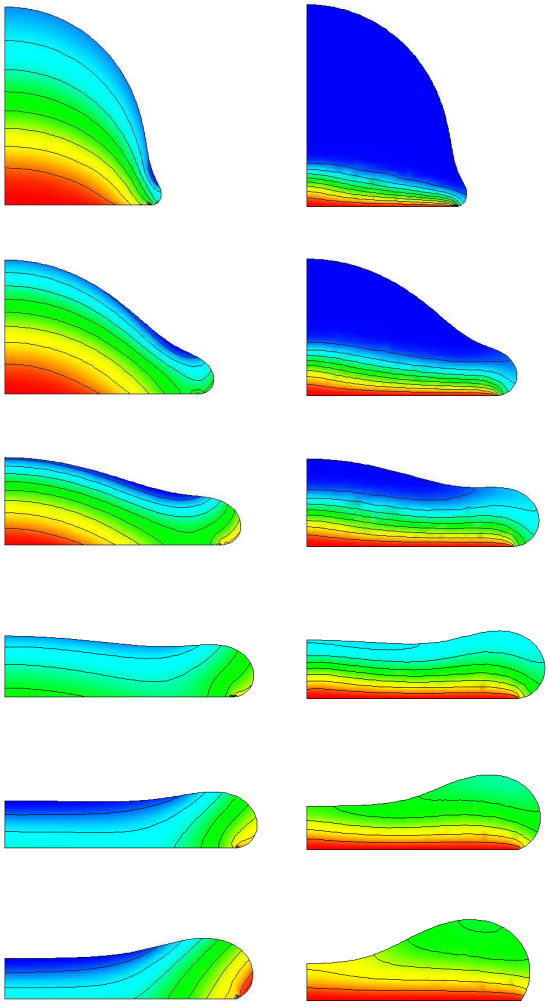

(i) (ii)

Figure 2: Sequence of images of liquid droplets with $\theta_e = 50^\circ$ obtained in different simulations. (i) without heat transfer effect, (ii) with heat transfer effect. Isolines in (i) and (ii) represent the pressure and temperature fields, respectively.

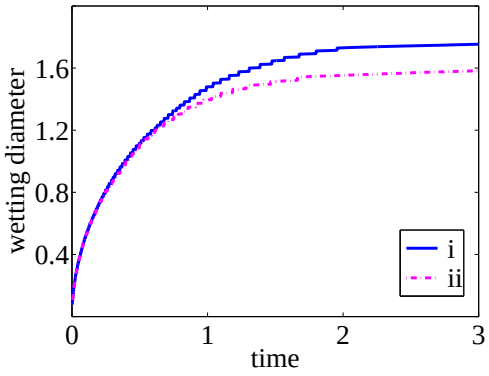

Figure 3: Wetting diameter of a liquid droplet impinging on a heated solid surface with $Re = 27$, $We = 24$, $Fr = 5$, $Pe = 27$, $Bi = 8.7 \times 10^{-6}$. (i) without heat transfer, (ii) with heat transfer.

For testing the algorithm, we stick our numerical study to small Peclet numbers. Extensions to higher Peclet numbers are possible by using stabilization techniques for the energy equations, see for example Matthies *et al.* (2006).

In the first test case, we used $T_w = 332.4^\circ$ K, $T_{sa} = 373^\circ$ K, $T_\infty = 283^\circ$ K (temperature of the solid surface, the saturation and the atmospheric, respectively), and the dimensionless numbers: $Re = 27$, $We = 24$, $Fr = 5$, $Pe = 27$, $Bi = 8.7 \times 10^{-6}$, $1/\beta_\epsilon = 1000$. The computationally obtained shapes of the 3D-axisymmetric droplet at different instances with and without heat transfer effects are plotted in Figure 2 (i) and (ii), respectively. The dimensionless timings from top to bottom are t =0.5, 1, 1.5, 2, 2.5, 3. The isolines in (i) and (ii) represent the pressure and temperature fields in the droplet, respectively. As we expected, effects of the temperature near the contact line region are large in comparison with other parts of the free surface. At later stage, a rim like structure is developed near the contact line and it counteracts with the spreading. This process slow down the wetting

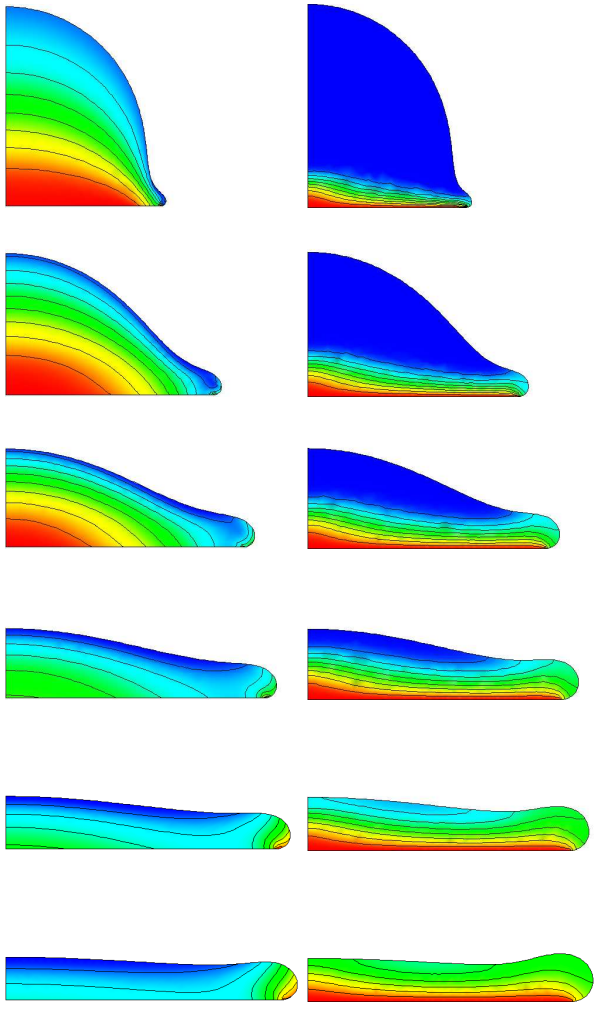

(i) (ii)

Figure 4: Sequence of images of liquid droplets with $\theta_e = 50^\circ$ obtained in different simulations. (i) without heat transfer effect, (ii) with heat transfer effect. Isolines in (i) and (ii) represent the pressure and temperature fields, respectively.

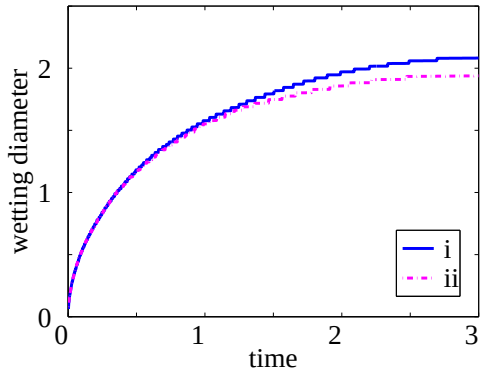

Figure 5: Wetting diameter of a liquid droplet impinging on a heated solid surface with $Re = 53$, $We = 97$, $Fr = 20$, $Pe = 53$ and $Bi = 8.7 \times 10^{-6}$. (i) without heat transfer, (ii) with heat transfer.

rate and reduce the maximal wetting diameter. These effects can be clearly seen in Figure 3, which represents the wetting diameter in time.

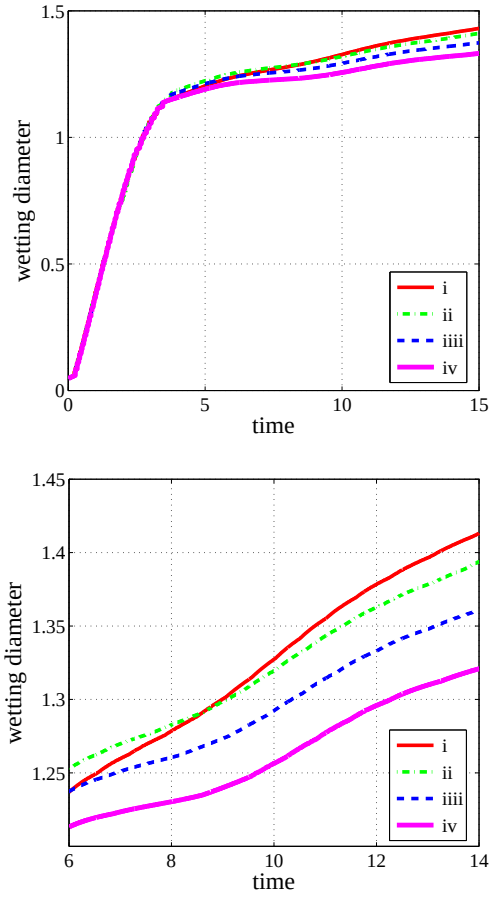

Figure 6: Wetting diameter (zoom in time (bottom)) of a liquid droplet impinging on a heated solid surface with $Re = 53$, $We = 97$, $Fr = 20$, $Pe = 53$ and $Bi = 8.7 \times 10^{-6}$ for different surface temperatures T_W, (i) 292, (ii) 312, (iii) 332 and (iv) 352.

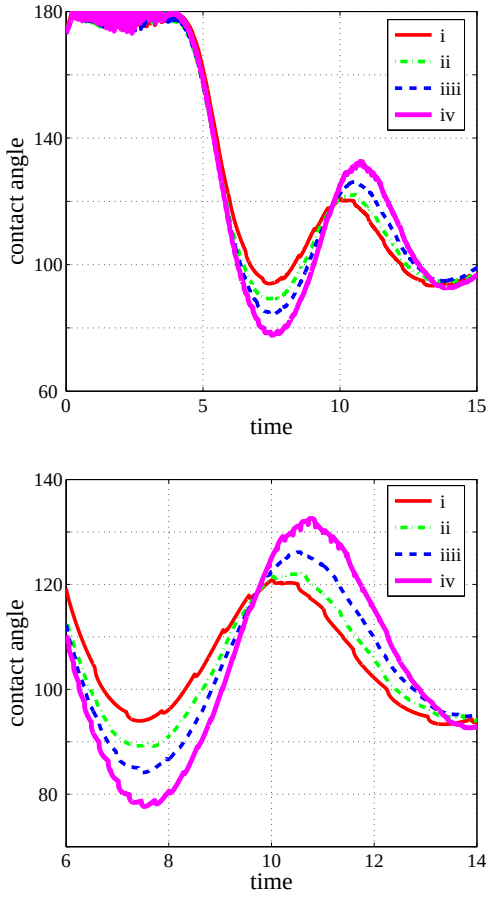

Figure 7: Dynamic contact angle (zoom in time (bottom)) of a liquid droplet impinging on a heated solid surface with $Re = 53$, $We = 97$, $Fr = 20$, $Pe = 53$ and $Bi = 8.7 \times 10^{-6}$ for different surface temperatures T_W, (i) 292, (ii) 312, (iii) 332 and (iv) 352.

Next, we perform another set of computations with a different set of dimensionless numbers: $Re = 53$, $We = 97$, $Fr = 20$, $Pe = 53$ and $Bi = 8.7 \times 10^{-6}$ with $T_w = 332.4°$ K, $T_{sa} = 373°$ K, $T_\infty = 283°$ K. The computationally obtained shapes of droplets for this test case at different instances with and without heat transfer are visualised in Figure 4 (i) and (ii), respectively. The dimensionless timings from top to bottom are t =0.5, 1, 1.5, 2, 2.5, 3. The isoline in (i) and (ii) represent the pressure and temperature fields in the droplet, respectively. The wetting diameter for this test case is presented in Figure 5. We observe a similar effect of the heat transfer as in the previous test case.

Next, to study the influence of the surface temperature, we performed an array of computations with T_w=292° K, 312° K, 332° K, and 352° K for a droplet with $Re = 27$, $We = 24$, $Fr = 5$, $Pe = 27$, $Bi = 8.7 \times 10^{-6}$, $1/\beta_\epsilon = 1000$. The wetting diameter and the dynamic contact angle obtained for these four different values of surface temperature are presented in Figure 6. Initially, for this particular set of data, there are almost no variations of the wetting diameter depending on the surface temperature. Nevertheless, a slight differences in the wetting diameter after time $t = 4$ can be

observed, see Figure 6 (bottom) for a closer view. These results show that the wetting diameter decreases when the surface temperature increases. Further, the influence of the surface temperature on the dynamics of the contact angle can be seen clearly in Figure 7. We observed that the dynamic contact angle increases when the solid surface temperature increases.

Concluding remarks

A mathematical model is presented for a non-isothermal deforming droplet with dynamic contact angle on a hot surface, which is below the boiling point temperature. The numerical study shows that the heat transfer slow down the spreading rate and the maximum value of the wetting diameter. However, to commend on the influence of other parameters such as the density, viscosity, surface tension, impact velocity and contact angles with respect to the heat transfer, further numerical investigations are needed.

Acknowledgements

The authors would like to thank the German research foundation for partially supporting this research through the Grant To143/9.

References

Anderson D. M. and Davis S. H. The spreading of volatile liquid droplets on heated surfaces. Phys. Fluids., Volume 7(2), 248 – 265 (1995)

Bänsch E. Numerical methods for the instationary Navier-Stokes equations with a free capillary surface. Habilitationsschrift, Albert-Ludwigs Universität (2001)

Behr M. and Abraham F. Free-surface flow simulations in the presence of inclined walls. Comp. Meth. in App. Mech. and Engrg, Volume 191(47-48), 5467 – 5483 (2002)

Davis T. A and Duff I. S. An unsymmetric-pattern multifrontal method for sparse LU factorization. SIAM Journal on Matrix Analysis and Applications, Volume 18(1), 140 – 158 (1997)

Davis T. A and Duff I. S. A combined unifrontal/multifrontal method for unsymmetric sparse matrices. ACM Transactions on Mathematical Software, Volume 25(1), 1-19 (1999)

Davis T. A. A column pre-ordering strategy for the unsymmetric-pattern multifrontal method. ACM Transactions on Mathematical Software, Volume 30(2), 165-195 (2004)

Davis T. A. Algorithm 832: UMFPACK, an unsymmetric-pattern multifrontal method. ACM Transactions on Mathematical Software, Volume 30(2), 196-199 (2004)

Dussan V E. B. The moving contact line: the slip boundary condition. Journal of Fluid Mechanics, 77(4), 665–684, (1976)

Dziuk G. An algorithm for evolutionary surfaces. Numer. Math., Volume 58, 603–611 (1991)

Eggers J. and Stone H. A. Characteristic lengths at moving contact lines for a perfectly wetting fluid: the influence of speed on the dynamic contact angle. J. Fluid Mech., Volume 505, 309 – 321 (2004)

Ganesan S. Finite element methods on moving meshes for free surface and interface flows. PhD Thesis, Fakultät für Mathematik, Otto-von-Guericke-Universität, Magdeburg, Published as book (ISBN 3-939665-06-1) by docupoint Verlag Magdeburg, (2006)

Harvie D. J. E. and Fletcher D. F. A hydrodynamic and thermodynamic simulation of droplet impacts on hot surfaces, part I: theoretical model. Int. J. of Heat and Mass Transfer, Volume 44, 2633 – 2642 (2001)

Hocking L. M. A moving fluid interface. part 2. the removal of the force singularity by a slip flow. J. Fluid Mech., Volume 79(2), 209 – 229 (1977)

Matthies G. Finite element methods for free boundary value problems with capillary surfaces. PhD thesis, Otto-von-Guericke-Universität, Fakultät für Mathematik, Magdeburg, Published as book (ISBN 978-3-8322-0863-3) by Shaker Verlag Aachen, (2002)

Matthies G., Skrzypacz P. and Tobiska. L. A unified convergence analysis for local projection stabilisations applied to the Oseen problem. Preprint 44/2006, Fakultät für Mathematik, Otto-von-Guericke-Universität, Magdeburg, (2006)

Ruschak K. A method for incorporating free boundaries with surface tension in finite element fluid-flow simulators. Int. J. Num. Meth. Engng., Volume 15, 639-648 (1980)

Šikalo Š., Wilhelm H.-D., Roisman I. V., Jakirlić S. and Tropea C. Dynamic contact angle of spreading droplets: Experiments and simulations. Physics of Fluids, 17(062103), 1–13, (2005)